Published online 8 June 2010

Nucleic Acids Research, 2010, Vol. 38, No. 19 ***6729–6736***
doi:10.1093/nar/gkq505

The crystal structure of an 'All Locked' nucleic acid duplex

André Eichert[1], Katja Behling[1], Christian Betzel[2], Volker A. Erdmann[1], Jens P. Fürste[1] and Charlotte Förster[1,*]

[1]Institute of Chemistry and Biochemistry, Free University Berlin, 14195 Berlin and [2]Institute of Biochemistry and Molecular Biology, Laboratory for Structural Biology of Infection and Inflammation, University of Hamburg, c/o DESY, 22603 Hamburg, Germany

Received April 21, 2010; Revised May 17, 2010; Accepted May 18, 2010

ABSTRACT

'Locked nucleic acids' (LNAs) are known to introduce enhanced bio- and thermostability into natural nucleic acids rendering them powerful tools for diagnostic and therapeutic applications. We present the 1.9 Å X-ray structure of an 'all LNA' duplex containing exclusively modified β-D-2′-*O*-4′*C*-methylene ribofuranose nucleotides. The helix illustrates a new type of nucleic acid geometry that contributes to the understanding of the enhanced thermostability of LNA duplexes. A notable decrease of several local and overall helical parameters like twist, roll and propeller twist influence the structure of the LNA helix and result in a widening of the major groove, a decrease in helical winding and an enlarged helical pitch. A detailed structural comparison to the previously solved RNA crystal structure with the corresponding base pair sequence underlines the differences in conformation. The surrounding water network of the RNA and the LNA helix shows a similar hydration pattern.

INTRODUCTION

Nucleic acids that are targeted against specific molecules in cellular metabolism like tumor markers, viruses or gene defects have great potential for applications in oligonucleotide-based drug design. These applications comprise diagnostic approaches and clinical therapies. There is a need for the stabilization of nucleic acids, since natural RNA and DNA molecules are highly sensitive against nuclease digestion and often possess low thermal stability. Great effort is spent in the development of modified oligonucleotides that maintain the Watson–Crick base pairing ability and tertiary structure interactions.

During the last years, special interest has been focused on nucleotide analogues that exhibit the N-type sugar puckering and possess the overall A-RNA-type conformation. Examples are 2′-alkylated RNAs like 2′-*O*-methyl-RNA (1), 2′-F-RNAs (2), phosphoramidate-RNAs (1) and the 'locked' nucleic acid family (3). A high increase in thermostability could be demonstrated for nucleic acids, which were substituted by locked nucleotide building blocks containing the 2′-*O*-4′*C*-methylene-β-D-ribofuranose (3). The melting temperature is increased by +2 to +10°C per LNA monomer in an oligoribonucleotide hybridized to RNA (3). A comparative study using different modifications in a nucleic acid could be demonstrated by substituting the Tenascin-C aptamer TTA-1 with several of the common modifications. The *in vitro* thermostability was described to be in the following order: 2′-F/2′-OMe < RNA/RNA ≤ 2′-OMe/2′-OMe < 2′-F/LNA < RNA/LNA < 2′-OMe/LNA < LNA/LNA (4).

LNAs are widely used in the field of nucleic acids research, covering a broad range of applications. For example, locked nucleic acid (LNA) building blocks are employed to improve targeting, specificity and stability of aptamers (4,5), utilized in DNAzymes to increase targeting and cleavage efficiency (6,7), used in miRNA silencing in direct antagonist (8) and LNAzyme approaches (9), functionalized as molecular beacons (10), applied to enhance RNA *in situ* hybridization (11,12), employed for transfectant-independent delivery of oligonucleotides (13) and used in antisense (7,14) and siRNA approaches (15,16).

A variety of structural investigations have been undertaken to analyze the structure and the conformation of nucleic acids, which were substituted by LNA building blocks. Also, LNA/DNA or LNA/RNA heteroduplexes have been investigated with respect to their 3D structure, their hybridization behavior and thermostability criteria. The studies could provide detailed information of the local geometric parameters of the mix-mer helices and of the

*To whom correspondence should be addressed. Tel: +49 30 83856023; Fax: +49 30 83856413; Email: foerster@chemie.fu-berlin.de

heteroduplexes. Structural investigations using 2′-*O*-4′*C*-methylene-β-D-ribofuranose LNA–RNA mix-mers hybridized to RNA showed that introduction of single LNA nucleotides in double strands maintains the RNA A-type nucleic acid conformation, whereas the use of α-L-2′-*O*-4′*C* ribofuranose LNA–DNA mix-mers hybridized to DNA helices results in the B-type geometry (17,18).

Coherent with these results, investigations of heteroduplexes consisting of fully modified LNA strands hybridized to either RNA or DNA, showed that the 2′-*O*-4′*C*-methylene-β-D-ribofuranose LNA strand bound to RNA adopts an A-RNA-type conformation, whereas the binding to DNA induces a mixed N- and S-type sugar puckering (19). Accordingly, the 2′-*O*-4′*C*-methylene-α-L-ribofuranose LNA binds to DNA in a B-DNA-type conformation (20). All structural studies show that the 2′-*O*-4′*C*-methylene-β-D-ribofuranose 'locks' the LNA in the C3′-endo conformation, which is discussed to influence the geometry of the phosphate backbone and to orient the duplex in a way towards a more efficient base stacking (3). Molecular dynamics simulations yielded first insights into an 'all LNA' duplex structure based upon these data (21). Our work, presented here, contributes to the understanding of this widely used class of molecules by providing the lacking piece of information in the series of RNA/RNA, RNA/LNA, LNA/LNA structure investigations and computer modellings.

Concerning the surrounding solvent water network in nucleic acids, it is well accepted that the extensive solvation of the minor groove in RNA molecules is governed by specific hydration of the ribose 2′-OH group (22). It is also nowadays understood that the hydration of RNA plays an important role in RNA–protein interactions and that the extensive solvent content of the minor groove has a special function for the respective RNA (23). For LNA, it is assumed that the 2′-oxygen atom of the 2′-*O*-4′*C*-methylene-β-D-ribofuranose is involved in the hydration of the minor groove (19). Molecular dynamics simulations provided a first insight into water structure and dynamics of an LNA duplex (21).

Here, we present the crystal structure of an 'all LNA' helix at 1.9 Å resolution. As we intended to undertake comparative crystallographic studies between LNA and RNA, the sequence was derived from a $tRNA^{Ser}$ acceptor stem microhelix, the structure of which has been solved recently to 1.2 Å resolution (24). The local and overall geometric parameters of the LNA helix reveal a novel nucleic acid conformation with geometric parameters different to those known for RNA or DNA. Furthermore, the hydration patterns for the comparable LNA and RNA crystal structures are presented.

MATERIALS AND METHODS

Crystallization and acquisition of X-ray diffraction data

The 7mer LNA helix was derived from the *Escherichia coli* $tRNA^{Ser}$ aminoacyl stem microhelix, which has been crystallized previously (24) and originated from the $tRNA^{Ser}$ isoacceptor with the data base ID: RS 1661 (25). For the comparative structure analysis, the LNA was constructed to contain exclusively LNA building blocks by maintaining the base sequence of the RNA, except the U to T and C to m^5C exchange in standard LNA synthesis. The LNA sequence 5′-(m^5C-m^5C-T-m^5C-A-m^5C-m^5C)^L-3′, 5′-(G-G-T-G-A-G-G)^L-3′ corresponds to the sequence of the natural RNA: 5′-(C-C-U-C-A-C-C)-3′, 5′-(G-G-U-G-A-G-G)-3′.

The sample preparation, LNA hybridization and the crystallization screening was performed as described previously (26). The best LNA crystals appeared after 3–4 days using the following procedure and conditions: 1 µl of the 0.5 mM aqueous LNA solution was used and combined with 1 µl 40 mM sodium cacodylate, pH 5.5, 20 mM cobalt hexamine, 80 mM sodium chloride, 20 mM magnesium chloride, 10% (v/v) 2-methyl-2,4-pentanediol (MPD) on a cover slide and equilibrated against 1 ml of 35% (v/v) MPD in Linbro Plates (ICN Biomedicals Inc., Ohio, USA) using the hanging drop vapour diffusion technique at 294 K (26). The X-ray diffraction data were recorded at the Elettra Synchrotron (Trieste, Italy) beam line XRD1 at a wavelength of 1.000 Å. We recorded data between 80 and 1.9 Å resolution, which were processed and scaled using the programs DENZO and SCALEPACK from the HKL-2000 package (27).

X-ray structure determination and refinement

As crystal disorder may occur within crystals of short oligonucleotides (28,29), we analyzed the data applying the Padilla and Yeates algorithm (30). The calculations showed the curve of a theoretically untwined crystal, so we had no indications for merohedral twinning. Molecular replacement calculations were performed using the program PHASER (31) within the CCP4i program suite (32). As a search model, we constructed an artificial LNA duplex by keeping the base sequence of the RNA, but replacing the natural ribonucleotides by standard LNA building blocks (Figure 1). Structure refinement was calculated with the program REFMAC (33) and calculation of electron density maps was performed with FFT (34). Both programs were used as implemented in the CCP4i package (32). *X3DNA* was applied for calculating the local and overall geometric parameters. Graphical representations were done with the programs PYMOL (www.pymol.org) and RASMOL (35).

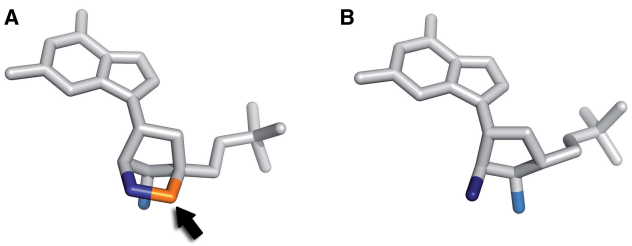

Figure 1. A guanosine nucleotide shown as LNA with the 2′-*O*-4′*C*-methylene-β-D-ribofuranose sugar moiety (**A**) and as RNA with the natural occurring ribose (**B**) The arrow indicates the 2′-*O*-4′*C*-methylene group (colored orange) in LNA nucleotides.

Melting curves

The melting curves of the $tRNA^{Ser}$ microhelix and the corresponding 'all LNA' duplex were recorded on a Hewlett Packard Diode Array spectrophotometer 8452A in the following buffer: 1.73 mM disodium hydrogen phosphate, 1mM potassium dihydrogen phosphate, pH 7.2, 100 mM sodium chloride and 0.1 mM EDTA at an RNA or LNA concentration of 5.0 μM. The absorption at 260 nm was measured as a function of temperature within a range of 10–90°C and steps of 1°C increase per minute. The T_m values were obtained from the maxima of the first derivatives of the melting curves.

RESULTS AND DISCUSSION

Crystallographic data and crystal packing

The crystallization of the LNA duplex has been reported previously (26). Within the molecular replacement calculations, the rotation function gave a *Z*-score of 9.6 and the translation function a *Z*-score of 18.5. As expected, according to the calculated Mathews coefficient and the solvent content (Table 1), we detected two LNA duplexes per asymmetric unit. No clashes could be recognized between symmetry-related molecules. The refinement calculations and the addition of solvent molecules, one magnesium ion, one cobalt hexamine and one cacodylate molecule dropped the initial R/R_{free} of 37.6/37.0% to final values of R/R_{free} 22.4/26.4% (Table 1). We detected 314 LNA atoms per single helix and a total of 100 solvent water molecules within the asymmetric unit. Since the geometrical parameters of all nucleotides show a high similarity (Supplementary Data), we conclude the lack of distortions at the ends of the investigated helices. An overall structure of the previously solved RNA helix with corresponding sequence and the LNA duplex structures are presented in Figure 2A. A representative 1.9 Å $2F_o$-F_c electron density map of the LNA structure is illustrated by showing the region of the base pair $(T_3–A_{70})^L$ with the β-D-2′-*O*-4′*C*-methylene ribofuranose moiety and several associated solvent molecules (Figure 2B).

Table 1. Data collection and refinement statistics

	LNA duplex crystal
Data collection	
Space group	*C*2
Cell dimensions	
a, *b*, *c* (Å)	77.91, 40.74, 30.06
α, β, γ (°)	90.00, 91.02, 90.00
Resolution (Å)	80.00–1.90 (1.93–1.90)
R_{merge}	7.3 (21.7)
$I / \sigma I$	19.7 (1.0)
Completeness (%)	98.0 (97.2)
Redundancy	4.8 (3.8)
Refinement	
Resolution (Å)	
Number of reflections	7382
R_{work}/R_{free}	22.4 (26.4)
Number of atoms/a.u.	
Nucleic acid	628
Magnesium	1
Cobalthexamine	1
Cacodylate	1
Water	100
B-factors	
LNA	30.9
Magnesium	18.4
Cobalthexamine	28.2
Cacodylate	86.1
Water	38.2
RMSD	
Bond lengths (Å)	0.016
Bond angles (°)	3.371

Values in parentheses are for highest-resolution shell.

The stacking of the two LNA helices is influenced by a cobalt hexamine (Figure 3A), which is located in the interface between the two duplexes. Two LNA helices in the asymmetric unit stack on top of each other building so-called endless rows of helices. The stacking behavior is in a 'tail-to-tail' manner, as the 3′-$(G_7 – m^5C_{66})^L$-5′ base pairs, which represent the lower ends of the helices, face each other. The cobalt hexamine is coordinated to the bases $(G_7)^L$ and $(G_6)^L$ of each duplex in a defined network of contacts. Four amino groups of the hexamine are directly coordinated to the exocyclic oxygen O6 and the endocyclic nitrogen N7 of the $(G_7)^L$ of both LNA helices. Two amino groups of the cobalt hexamine contact the $(G_6)^L$ nucleotides of both strands either *via* a bridging water molecule or directly to the exocyclic oxygen O6 and the endocyclic nitrogen N7. In summary, the crystal packing of the LNA duplexes is favored by hydrophobic interactions of the 'tail-to-tail' guanosine stacking and is further facilitated by interactions with the cobalt hexamine, which acts like a bridge between the two helices. A comparison of the crystallographic parameters between the previously solved RNA structure (24) and the here presented LNA structure demonstrates significant differences in crystal packing, although the RNA and LNA crystallize under identical conditions (24,26). The $tRNA^{Ser}$ microhelix crystallizes with one RNA helix per asymmetric unit, whereas the molecule packing consists of two molecules per asymmetric unit for the LNA duplex. The diffraction limit for the RNA crystals showed a resolution of 1.2 Å compared to 1.9 Å for the LNA data. In addition, the pattern of metal bindings differ, as the RNA revealed two magnesium binding sites, whereas the LNA complexes one cobalt hexamine, one magnesium ion and a cacodylate molecule.

Structure and conformation of the LNA duplex

The crystal structure of the 'all LNA' 7mer helix presents a nucleic acid geometry that cannot be compared to the canonical A- and B-type nucleic acid conformations. The LNA duplex geometry can rather be brought in vicinity to the structures of glycol nucleic acids (36), peptide nucleic acids (PNAs) (37) or Homo-DNA (38). We can describe the LNA duplex as a right-handed antiparallel helix maintaining the Watson–Crick base pairing and a 2′-exo conformation for all nucleotides. Nevertheless, the LNA possesses overall helical parameters that induce a

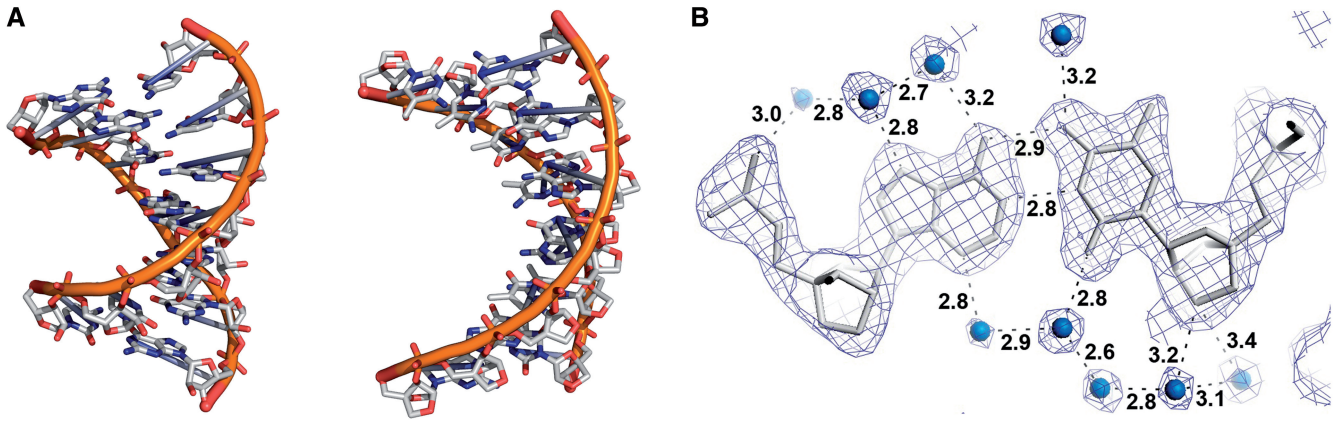

Figure 2. (**A**) Overall crystal structures of the RNA helix (24) (3gvn.pdb, left) and the LNA helix (2x2q.pdb, right) (**B**) Representative $2F_o$-F_c electron density map of the 'all locked' LNA duplex at 1.9 Å resolution showing the base pair (T3-A70)^L. Water molecules are presented by blue dots and distances are pointed out in Å.

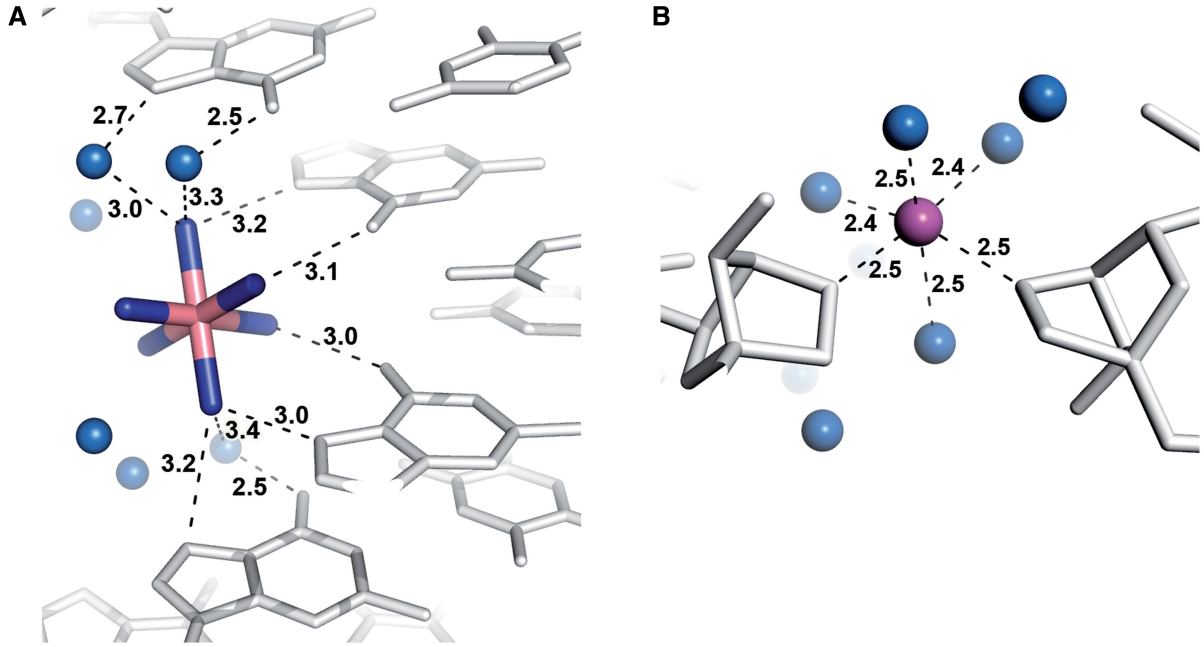

Figure 3. Metal ion binding sites in the LNA duplex. (**A**) The cobalt hexamine acts as an 'anchor' between the two duplexes in the asymmetric unit. The amino groups of the cobalt hexamine contact the guanosine nucleotides either directly or via water molecules. (**B**) The hexacoordinated magnesium ion is associated to water molecules and to the bridged 2′-oxygen of two symmetry equivalent 2′-*O*-4′*C*-methylene-β-D-ribofuranose sugars.

non-standard nucleic acid geometry. The predominant features of the LNA helix geometry comprise deviations in the local and overall helical parameters (Table 2). Compared to RNA helices, we detected a decrease in the helical twist, roll and propeller twist. The helical LNA twist shows average values of 26°, instead of 32° as known for RNA. The roll is decreased from 7–8° to ~4° and the propeller twist is decreased from 10–12° to ~7°. These parameters facilitate a widening of the major groove, which shows values of 24–25 Å in diameter, as compared to 16 Å observed for a standard A-RNA duplex. On the other hand, the LNA minor groove comprises 15 Å in diameter as compared to the 19 Å found for RNA. All values for slide and rise are slightly increased in the LNA structure. The altered geometric parameters induce a large hollow cave in the middle of the duplex viewing down the helical axis. In LNA, with a twist of 26° we observed 14 bp per turn as compared to 11 bp per turn in RNA. Due to the enlarged helical rise of 3.2 Å and the unwinding of the helix resulting from the decreased twist angles, the LNA possesses a pitch of 39 Å instead of 29 Å for RNA (Table 3).

The backbone torsion angles of the LNA duplex resemble the values of RNA-type nucleic acids and fall into the sc^-, ap^+, sc^+, sc^+ ap and sc^- conformation (for the angles α, β, γ, δ, ε, ζ). The χ-values around the glycosidic bond show a high conformity and have the ap^+ conformation. As expected, all sugar residues in the LNA

Table 2. Overall geometric helical parameters of selected helices (i) $tRNA^{Phe}$ microhelix, generated from yeast $tRNA^{Phe}$ (1ehz.pdb) (40), (ii) $tRNA^{Ser}$ microhelix (3gvn.pdb) (24), (iii) RNA-LNA hybrid (1h0q.pdb) (19), (iv) the 'all LNA' duplex, represented by the two duplexes per asymmetric unit (2x2q.pdb)

	Twist (°)	Rise (Å)	Slide (°)	Roll (Å)	χ-Disp (Å)	P.Twist (°)
Generated $tRNA^{Phe}$ microhelix	32.54 ± 7.23	2.67 ± 0.24	−1.47 ± 0.24	8.42 ± 1.46	−3.97 ± 1.05	−12.17 ± 6.73
$tRNA^{Ser}$ microhelix	32.46 ± 3.76	2.64 ± 0.27	−1.68 ± 0.34	6.61 ± 1.80	−4.25 ± 1.25	−10.46 ± 4.95
1H0Q LNA–RNA hybrid	28.98 ± 4.06	2.72 ± 0.11	−2.24 ± 0.24	6.07 ± 6.03	−5.40 ± 0.88	−12.84 ± 3.64
LNA 1 $tRNA^{Ser}$ microhelix	25.97 ± 1.49	2.81 ± 0.04	−2.49 ± 0.24	4.08 ± 1.67	−6.60 ± 0.43	−6.65 ± 3.91
LNA 2 $tRNA^{Ser}$ microhelix	26.13 ± 1.53	2.84 ± 0.05	−2.47 ± 0.21	4.15 ± 2.23	−6.47 ± 0.43	−7.45 ± 2.84

All data were calculated using the program '3DNA' (41). χ-Disp. is the abbreviation for χ-Displacement and P.Twist is the Propellertwist.

Table 3. Average helical parameters for artificially constructed RNA as compared to the RNA/LNA duplex (1h0q.pdb) (19) and the 'all LNA' duplex (2x2q.pdb)

	BP/Turn	Twist (°)	Rise (Å)	Pitch (Å)
RNA	11	32	2.6	29
RNA/LNA	12	29	2.7	32
LNA	14	26	2.8	39

crystal structure are distributed in the 2′-exo conformation. The stability of the backbone in the LNA helix is a consequence of the chemical properties of the 2′-*O*-4′*C*-methylene-β-D-ribofuranose moiety, as this sugar is known to 'lock' the molecule in the 2′-exo conformation (3). The alteration of the geometric helical parameters of the LNA helix apparently induces a more efficient base stacking, as several values like twist, roll and propeller twist are decreased and lead to a more efficient hydrophobic interaction between the bases. This geometric arrangement results in a predominant enlargement of the major groove in coherence with a decrease of the minor groove and an enlarged pitch, maintaining the canonical Watson–Crick base pairing.

Hydration of the LNA duplex

The extensive hydration of the RNA minor groove is facilitated by the specific hydration of the ribose 2′-OH group (22). We investigated the arrangement of water molecules in the LNA duplex with special interest focused on the environment of the 2′-*O*-4′*C*-methylene-β-D-ribofuranose. We present a snapshot of hydrated nucleotides in the LNA as compared to the corresponding RNA (Figure 4). The first base pair, (G1-m^5C72)^L, shows a similar hydration of the LNA minor groove as known for RNA (Figure 4A). Water oxygen atoms contact the exocyclic O2 of the cytidin and the N3 and N4 of the guanosine by concomitant building of a network to the solvent molecule. Contacts are facilitated by 2′-oxygen of the guanosine LNA sugar. In analogy, another solvent molecule that is involved in the water network is in contact to the 2′-oxygen of the cytidine. The distribution of water molecules in the minor groove of the LNA duplex follows the general pattern of RNA hydration, as can also be demonstrated for the base pairs (G4-m^5C69)^L (Figure 4A) and (G2-m^5C71)^L (Figure 4B). The solvent molecules interact in an RNA-like fashion with the 2′-oxygen of the 2′-*O*-4′*C*-methylene-β-D-ribofuranose, which serves as a hydrogen acceptor similar to the 2′-OH group in RNA. The presence of the 2′-oxygen in the 2′-*O*-4′*C*-methylene-β-D-ribofuranose sugars in LNA helices allows the specific arrangement of water networks and allows an extensive hydration of LNAs as commonly described for RNA molecules (22). A direct comparison between LNA and RNA hydration is demonstrated in Figure 4B, where we exemplarily present the hydration of the LNA (m^5C2-G71)^L base pair and the corresponding region in the RNA structure, C2-G71.

The distribution of water molecules in the major groove of the LNA follows the general pattern of RNA hydration as well. Since we focused our interest on the hydration of 2′-oxygen atoms, we present pictures of base pairs with complete solvent saturation within the minor groove. However, we also observe a similar hydration pattern between LNA and RNA major grooves within other base pairs (data not shown) that display a more complete distribution of water oxygen atoms for this region.

Thermostability data

As has been reviewed, an increase of +2 to +10°C can be observed per LNA building block added in RNA strands hybridized to RNA (3). We investigated the thermostability of the 'all LNA' duplex and the corresponding RNA duplex by measuring the melting curves. The RNA 7mer homo duplex with the sequence 5′-(C-C-U-C-A-C-C)-3′ / 5′-(G-G-U-G-A-G-G)-3′ shows a T_m of 45°C, whereas the LNA with the corresponding base sequence 5′-(m^5C-m^5C-T-m^5C-A-m^5C-m^5C)^L-3′ / 5′-(G-G-T-G-A-G-G)^L-3′ possesses a T_m of >90°C, which is above the range of a feasible measurement. This is consistent with the so far published and reviewed observations (3), as the investigated LNA duplex here showed an increase in the melting temperature of >4°C per LNA building block.

CONCLUSIONS

The summative increase in the melting temperature of RNA duplexes by subsequent introduction of LNA building blocks and the maintenance of Watson–Crick base pairing properties of LNA/RNA duplexes highlights the LNAs as powerful tools in therapeutic and diagnostic applications (39).

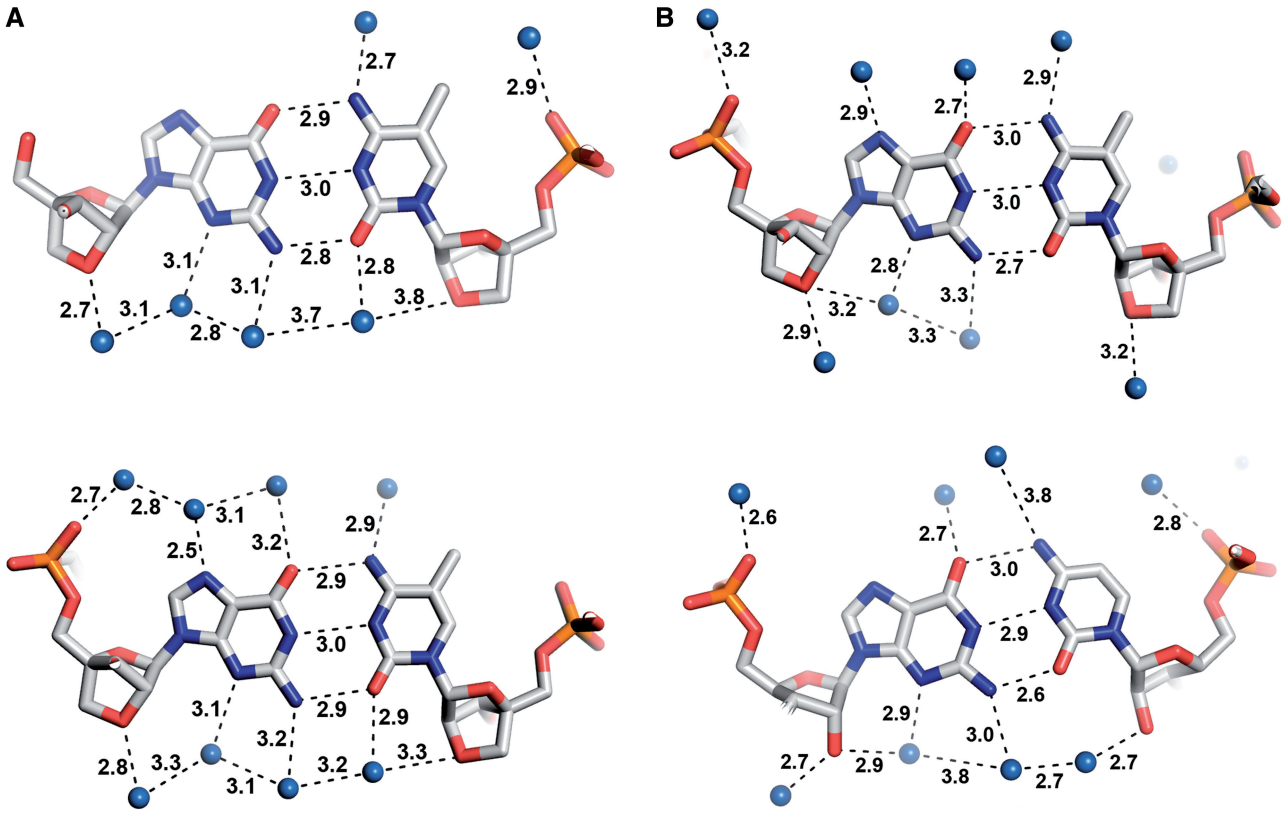

Figure 4. The hydration of LNA as demonstrated by the base pairs (**A**) (G1-m^{5}C72)^L (top) and (G4-m^{5}C69)^L (bottom). (**B**) Comparison of hydration in the LNA and RNA duplex by showing the LNA base pair (G2-m^{5}C71)^L (top) and the corresponding RNA base pair G2-C71 (bottom). Water oxygen atoms are presented by blue dots and distances are pointed out in Å. For better comparability, numbering of LNA bases was chosen to be identical to the tRNA-derived RNA sequence.

The LNA duplex crystal structure, presented here, reveals a nucleic acid conformation, which differs significantly from the canonical A- and B-type nucleic acid geometries. In order to clarify the helical differences between RNA, the RNA/LNA heteroduplex and the LNA duplex, we extended the helices to a maximum of 28 bp by taking advantage of the regular helical structure of nucleic acids, as done previously (36,37). We present the overall geometry by side view and top view in a Calladine–Drew Plot (Figure 5A). Additionally, the space filling models were elongated to a length of 46 bp (Figure 5B). The LNA duplex structure can be characterized as a 'stretched helix' with an extended major groove that goes in coherence with a decrease in the dimensions of the minor groove and an enlarged helical pitch. The LNA duplex possesses roughly 14 bp per helical turn in contrast to the 11 bp per turn in RNA (Table 3). The decrease in helical parameters like twist, roll, propeller twist and the partially observed interstrand stacking in the LNA duplex result in improved hydrophobic interactions between the bases and thereby increase the stacking energies of the nucleotides. As nucleobases possess conjugated double bonds, we interpret that the unwinding of the LNA helix as compared to RNA enlarges the sum of all π–π interactions within the stacked nucleotides by concomitantly maintaining the strong Van der Waals bonding between the surfaces of the bases. The sugar residues in the LNA duplex all lie in the 2′-exo conformation that is a property of the A-type nucleic acid geometry. Also, the phosphate and backbone arrangement in the LNA helix resembles that of an A-type structure. This is in concert with previously published results, as the chemical properties of the 2′-*O*-4′*C*-methylene-β-D-ribofuranose moiety are known to 'lock' the structures into the 2′-exo conformation (3,39). Furthermore, we can confirm and extend the findings of a previously published molecular dynamics simulation of LNAs (21). The LNA's helical parameters are similar in both, the computer-based and the crystallographic studies, resulting in a unique LNA conformation.

Interestingly, the structure of an RNA/LNA heteroduplex (17) is a geometric intermediate between the RNA and the 'all LNA' conformation (Tables 2 and 3; Figure 5). There is a consecutive order in the structural changes from the geometry of an RNA duplex *via* the conformation of an RNA/LNA heteroduplex to the fold of an 'all LNA' duplex.

ACCESSION NUMBERS

Protein data bank: coordinates and structure factors for the LNA duplex, derived from the tRNA^{Ser} microhelix, have been deposited with the accession code 2X2Q.PDB.

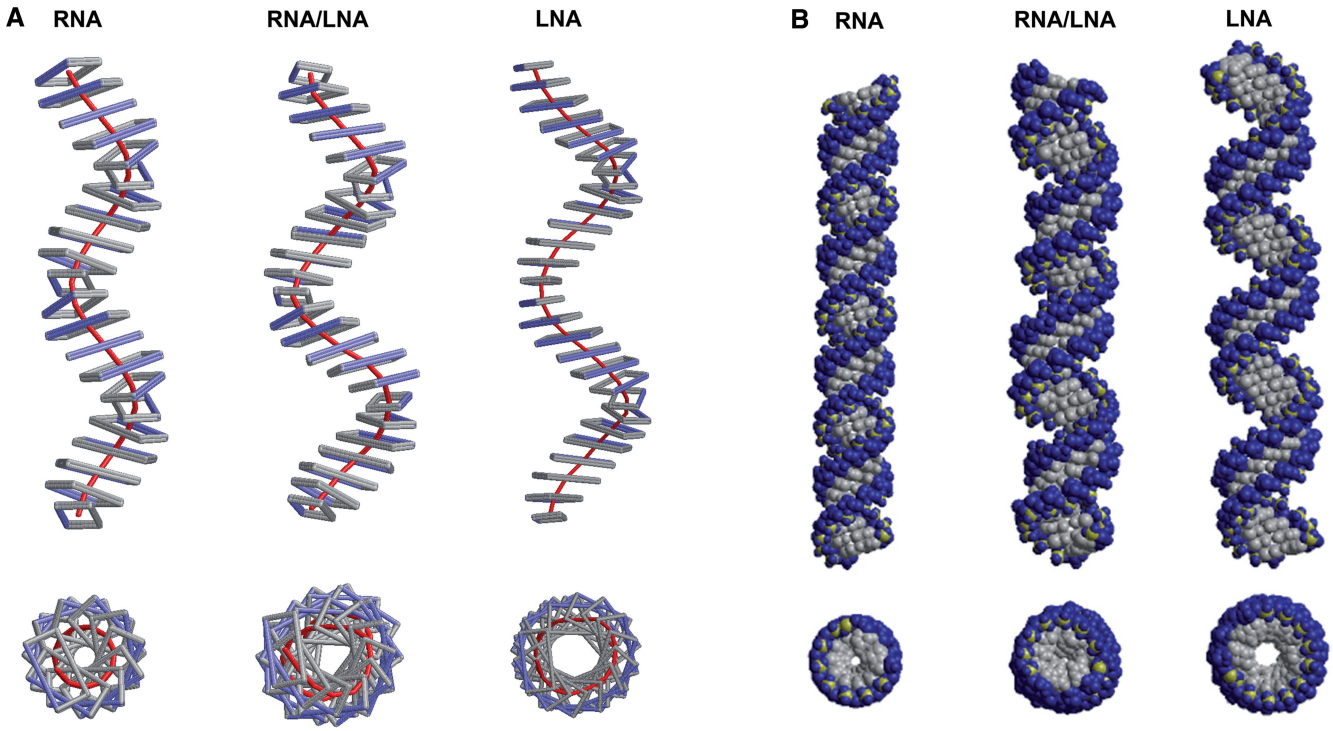

Figure 5. Calladine–Drew plot (**A**) of idealized RNA, the RNA/LNA hybrid (derived from 1h0q.pdb) and the LNA (2x2q.pdb) with two helical turns each. Left: RNA (22 bp), middle: RNA/LNA (25 bp) and right: LNA (28 bp). Base pairs are presented as gray–blue rectangles and the helical winding is pointed out by the curved red line. Side view (top) and top view (bottom). Space filling models of the same helices (**B**) with 46 bp per duplex. Details are described in the text.

SUPPLEMENTARY DATA

Supplementary Data are available at NAR Online.

ACKNOWLEDGEMENTS

We gratefully acknowledge the ELETTRA synchrotron facility, Trieste, Italy, for providing beam time. A.E. is member of the Dahlem Research School of the Freie Universität Berlin.

FUNDING

Deutsches Zentrum für Luft- und Raumfahrt; Bundesministerium für Bildung und Forschung (to BiGRUDI network of the Robert Koch-Institut, Berlin). Friedrich-Ebert-Stiftung, Germany (to A.E.). Funding for open access charge: The BiGRUDI network of the Robert Koch-Institut and the EU via the Network OptiCryst, LSHG-CT-2006-037793 (Contract No. 037793).

Conflict of interest statement. None declared.

REFERENCES

1. Manoharan,M. (1999) 2′-Carbohydrate modifications in antisense oligonucleotide therapy: importance of conformation, configuration and conjugation. *Biochim. Biophys. Acta*, **1489**, 117–130.
2. Kawasaki,A.M., Casper,M.D., Freier,S.M., Lesnik,E.A., Zounes,M.C., Cummins,L.L., Gonzalez,C. and Cook,P.D. (1993) Uniformly modified 2′-deoxy-2′-fluoro phosphorothioate oligonucleotides as nuclease-resistant antisense compounds with high affinity and specificity for RNA targets. *J. Med. Chem.*, **36**, 831–841.
3. Petersen,M. and Wengel,J. (2003) LNA: a versatile tool for therapeutics and genomics. *Trends Biotechnol.*, **21**, 74–81.
4. Schmidt,K.S., Borkowski,S., Kurreck,J., Stephens,A.W., Bald,R., Hecht,M., Friebe,M., Dinkelborg,L. and Erdmann,V.A. (2004) Application of locked nucleic acids to improve aptamer in vivo stability and targeting function. *Nucleic Acids Res.*, **32**, 5757–5765.
5. Darfeuille,F., Reigadas,S., Hansen,J.B., Orum,H., Di,P.C. and Toulme,J.J. (2006) Aptamers targeted to an RNA hairpin show improved specificity compared to that of complementary oligonucleotides. *Biochemistry*, **45**, 12076–12082.
6. Vester,B., Lundberg,L.B., Sorensen,M.D., Babu,B.R., Douthwaite,S. and Wengel,J. (2002) LNAzymes: incorporation of LNA-type monomers into DNAzymes markedly increases RNA cleavage. *J. Am. Chem. Soc.*, **124**, 13682–13683.
7. Jakobsen,M.R., Haasnoot,J., Wengel,J., Berkhout,B. and Kjems,J. (2007) Efficient inhibition of HIV-1 expression by LNA modified antisense oligonucleotides and DNAzymes targeted to functionally selected binding sites. *Retrovirology*, **4**, 29.
8. Elmen,J., Lindow,M., Schutz,S., Lawrence,M., Petri,A., Obad,S., Lindholm,M., Hedtjarn,M., Hansen,H.F., Berger,U. *et al.* (2008) LNA-mediated microRNA silencing in non-human primates. *Nature*, **452**, 896–899.
9. Jadhav,V.M., Scaria,V. and Maiti,S. (2009) Antagomirzymes: oligonucleotide enzymes that specifically silence microRNA function. *Angew. Chem. Int. Ed. Engl.*, **48**, 2557–2560.
10. Wang,L., Yang,C.J., Medley,C.D., Benner,S.A. and Tan,W. (2005) Locked nucleic acid molecular beacons. *J. Am. Chem. Soc.*, **127**, 15664–15665.
11. Thomsen,R., Nielsen,P.S. and Jensen,T.H. (2005) Dramatically improved RNA in situ hybridization signals using LNA-modified probes. *RNA*, **11**, 1745–1748.
12. Wienholds,E., Kloosterman,W.P., Miska,E., Alvarez-Saavedra,E., Berezikov,E., de Bruijn,E., Horvitz,H.R., Kauppinen,S. and

Plasterk,R.H. (2005) MicroRNA expression in zebrafish embryonic development. *Science*, **309**, 310–311.
13. Stein,C.A., Hansen,J.B., Lai,J., Wu,S., Voskresenskiy,A., Hog,A., Worm,J., Hedtjarn,M., Souleimanian,N., Miller,P. *et al.* (2010) Efficient gene silencing by delivery of locked nucleic acid antisense oligonucleotides, unassisted by transfection reagents. *Nucleic Acids Res.*, **38**, e3.
14. Wahlestedt,C., Salmi,P., Good,L., Kela,J., Johnsson,T., Hokfelt,T., Broberger,C., Porreca,F., Lai,J., Ren,K. *et al.* (2000) Potent and nontoxic antisense oligonucleotides containing locked nucleic acids. *Proc. Natl Acad. Sci. USA*, **97**, 5633–5638.
15. Braasch,D.A., Jensen,S., Liu,Y., Kaur,K., Arar,K., White,M.A. and Corey,D.R. (2003) RNA interference in mammalian cells by chemically-modified RNA. *Biochemistry*, **42**, 7967–7975.
16. Elmen,J., Thonberg,H., Ljungberg,K., Frieden,M., Westergaard,M., Xu,Y., Wahren,B., Liang,Z., Orum,H., Koch,T. *et al.* (2005) Locked nucleic acid (LNA) mediated improvements in siRNA stability and functionality. *Nucleic Acids Res.*, **33**, 439–447.
17. Petersen,M., Bondensgaard,K., Wengel,J. and Jacobsen,J.P. (2002) Locked nucleic acid (LNA) recognition of RNA: NMR solution structures of LNA:RNA hybrids. *J. Am. Chem. Soc.*, **124**, 5974–5982.
18. Vester,B. and Wengel,J. (2004) LNA (locked nucleic acid): high-affinity targeting of complementary RNA and DNA. *Biochemistry*, **43**, 13233–13241.
19. Nielsen,K.E., Rasmussen,J., Kumar,R., Wengel,J., Jacobsen,J.P. and Petersen,M. (2004) NMR studies of fully modified locked nucleic acid (LNA) hybrids: solution structure of an LNA:RNA hybrid and characterization of an LNA:DNA hybrid. *Bioconjug. Chem.*, **15**, 449–457.
20. Nielsen,K.M., Petersen,M., Hakansson,A.E., Wengel,J. and Jacobsen,J.P. (2002) alpha-L-LNA (alpha-L-ribo configured locked nucleic acid) recognition of DNA: an NMR spectroscopic study. *Chemistry*, **8**, 3001–3009.
21. Pande,V. and Nilsson,L. (2008) Insights into structure, dynamics and hydration of locked nucleic acid (LNA) strand-based duplexes from molecular dynamics simulations. *Nucleic Acids Res.*, **36**, 1508–1516.
22. Auffinger,P. and Westhof,E. (1998) Hydration of RNA base pairs. *J. Biomol. Struct. Dyn.*, **16**, 693–707.
23. Draper,D.E. (1999) Themes in RNA-protein recognition. *J. Mol. Biol.*, **293**, 255–270.
24. Eichert,A., Fürste,J.P., Schreiber,A., Perbandt,M., Betzel,C., Erdmann,V.A. and Förster,C. (2009) The 1.2A crystal structure of an E. coli $tRNA^{Ser}$ acceptor stem microhelix reveals two magnesium binding sites. *Biochem. Biophys. Res. Commun.*, **386**, 368–373.
25. Sprinzl,M. and Vassilenko,K.S. (2005) Compilation of tRNA sequences and sequences of tRNA genes. *Nucleic Acids Res.*, **33**, D139–D140.
26. Behling,K., Eichert,A., Fürste,J.P., Betzel,C., Erdmann,V.A. and Förster,C. (2009) Crystallization and X-ray diffraction analysis of an 'all-locked' nucleic acid duplex derived from a $tRNA^{Ser}$ microhelix. *Acta Crystallogr. Sect. F Struct. Biol. Cryst. Commun.*, **65**, 809–812.
27. Otwinowski,Z. and Minor,W. (1997) Processing of X-ray diffraction data collected in oscillation mode. *Methods in Enzymology, Macromolecular Crystallography, part A*, **276**, 307–326.
28. Mueller,U., Muller,Y.A., Herbst-Irmer,R., Sprinzl,M. and Heinemann,U. (1999) Disorder and twin refinement of RNA heptamer double helices. *Acta Crystallogr. D Biol. Crystallogr.*, **55**, 1405–1413.
29. Rypniewski,W., Vallazza,M., Perbandt,M., Klussmann,S., Delucas,L.J., Betzel,C. and Erdmann,V.A. (2006) The first crystal structure of an RNA racemate. *Acta Crystallogr. D Biol. Crystallogr.*, **62**, 659–664.
30. Padilla,J.E. and Yeates,T.O. (2003) A statistic for local intensity differences: robustness to anisotropy and pseudo-centering and utility for detecting twinning. *Acta Crystallogr. D*, **59**, 1124–1130.
31. McCoy,A.J., Grosse-Kunstleve,R.W., Adams,P.D., Winn,M.D., Storoni,L.C. and Read,R.J. (2007) Phaser crystallographic software. *J. Appl. Crystallogr.*, **40**, 658–674.
32. Collaborative Computational Project and Number 4. (1994) "The CCP4 suite: programs for protein crystallography". *Acta Crystallogr*, **D50**, 760–763.
33. Murshudov,G.N., Vagin,A.A. and Dodson,E.J. (1997) Refinement of macromolecular structures by the maximum-likelihood method. *Acta Crystallogr. D Biol. Crystallogr.*, **53**, 240–255.
34. Read,R.J. and Schierbeek,A.J. (1988) A phased translation function. *J. Appl. Cryst.*, **21**, 490–495.
35. Sayle,R.A. and Milner-White,E.J. (1995) RASMOL: biomolecular graphics for all. *Trends Biochem. Sci.*, **20**, 374.
36. Schlegel,M.K., Essen,L.O. and Meggers,E. (2008) Duplex structure of a minimal nucleic acid. *J. Am. Chem. Soc.*, **130**, 8158–8159.
37. Rasmussen,H., Kastrup,J.S., Nielsen,J.N., Nielsen,J.M. and Nielsen,P.E. (1997) Crystal structure of a peptide nucleic acid (PNA) duplex at 1.7 A resolution. *Nat. Struct. Biol.*, **4**, 98–101.
38. Egli,M., Pallan,P.S., Pattanayek,R., Wilds,C.J., Lubini,P., Minasov,G., Dobler,M., Leumann,C.J. and Eschenmoser,A. (2006) Crystal structure of homo-DNA and nature's choice of pentose over hexose in the genetic system. *J. Am. Chem. Soc.*, **128**, 10847–10856.
39. Kaur,H., Babu,B.R. and Maiti,S. (2007) Perspectives on chemistry and therapeutic applications of Locked Nucleic Acid (LNA). *Chem. Rev.*, **107**, 4672–4697.
40. Shi,H. and Moore,P.B. (2000) The crystal structure of yeast phenylalanine tRNA at 1.93 A resolution: a classic structure revisited. *RNA*, **6**, 1091–1105.
41. Lu,X.J. and Olson,W.K. (2003) 3DNA: a software package for the analysis, rebuilding and visualization of three-dimensional nucleic acid structures. *Nucleic Acids Res.*, **31**, 5108–5121.